Translational Oncology
www.transonc.com

Volume 2 Number 4 December 2009 pp. 271–280 271

Multiparametric Characterization of Grade 2 Glioma Subtypes Using Magnetic Resonance Spectroscopic, Perfusion, and Diffusion Imaging[1]

Wei Bian*, Inas S. Khayal*,†, Janine M. Lupo*, Colleen McGue*, Scott Vandenberg‡, Kathleen R. Lamborn§, Susan M. Chang§, Soonmee Cha*,§ and Sarah J. Nelson*,†,¶

*Department of Radiology and Biomedical Imaging, University of California, San Francisco, CA, USA; †UCSF/UCB Joint Graduate Group in Bioengineering, University of California, San Francisco, CA, USA; ‡Department of Pathology, University of California, San Francisco, CA, USA; §Department of Neurological Surgery, University of California, San Francisco, CA, USA; ¶Department of Bioengineering and Therapeutic Science, University of California, San Francisco, CA, USA

Abstract

BACKGROUND AND PURPOSE: The purpose of this study was to derive quantitative parameters from magnetic resonance (MR) spectroscopic, perfusion, and diffusion imaging of grade 2 gliomas according to the World Health Organization and to investigate how these multiple imaging modalities can contribute to evaluating their histologic subtypes and spatial characteristics. *MATERIALS AND METHODS:* MR spectroscopic, perfusion, and diffusion images from 56 patients with newly diagnosed grade 2 glioma (24 oligodendrogliomas, 18 astrocytomas, and 14 oligoastrocytomas) were retrospectively studied. Metabolite intensities, relative cerebral blood volume (rCBV), and apparent diffusion coefficient (ADC) were statistically evaluated. *RESULTS:* The 75th percentile rCBV and median ADC were significantly different between oligodendrogliomas and astrocytomas ($P < .0001$) and between oligodendrogliomas and oligoastrocytomas ($P < .001$). Logistic regression analysis identified both 75th percentile rCBV and median ADC as significant variables in the differentiation of oligodendrogliomas from astrocytomas and oligoastrocytomas. Group differences in metabolite intensities were not significant, but there was a much larger variation in the volumes and maximum values of metabolic abnormalities for patients with oligodendroglioma compared with the other tumor subtypes. *CONCLUSIONS:* Perfusion and diffusion imaging provide quantitative MR parameters that can help to differentiate grade 2 oligodendrogliomas from grade 2 astrocytomas and oligoastrocytomas. The large variations in the magnitude and spatial extent of the metabolic lesions between patients and the fact that their values are not correlated with the other imaging parameters indicate that MR spectroscopic imaging may provide complementary information that is helpful in targeting therapy, evaluating residual disease, and assessing response to therapy.

Translational Oncology (2009) 2, 271–280

Introduction

Grade 2 gliomas are low-grade brain tumors that are diffusely infiltrating, slow-growing, and seen primarily in younger patients [1]. They comprise three major subtypes of tumors: oligodendrogliomas, oligoastrocytomas, and astrocytomas. Accurate characterization of these subtypes has its clinical importance in that they have different prognosis and response to therapy. Clinical observations have shown that oligodendrogliomas are more likely to respond to chemotherapy

Address all correspondence to: Wei Bian, University of California, San Francisco, Department of Radiology and Biomedical Imaging, Byers Hall, Suite 303, MC 2532, 1700 4th St, San Francisco, CA 94158-2330. E-mail: wei.bian@radiology.ucsf.edu

[1]This study was supported by National Institutes of Health grants R01 CA059880, R01 CA116041, PO1 CA 118816, and SPORE P50 CA97257.
Received 8 July 2009; Revised 8 July 2009; Accepted 13 July 2009

DOI 10.1593/tlo.09178

and patients with these tumors have better treatment outcome and longer survival times than patients with astrocytomas and oligoastrocytomas [2–4]. The diagnosis and classification of grade 2 gliomas currently rely on the histopathologic examination of biopsy specimens, but variations in tissue sampling for these heterogeneous tumors and restrictions on surgical accessibility make it difficult to be sure that the samples obtained are representative of the entire tumor [5].

Anatomic magnetic resonance (MR) imaging of the brain provides excellent soft tissue contrast and is routinely used for the noninvasive assessment of brain tumors, but its ability to define tumor type and grade of gliomas is limited [6]. New MR imaging modalities such as proton MR spectroscopic imaging (MRSI), perfusion-weighted imaging (PWI), and diffusion-weighted imaging (DWI) have been proposed as alternate methods for characterizing such tumors [7]. MRSI provides an assessment of the metabolic signature of brain tumors [8–10]. PWI measures relative cerebral blood volume (rCBV), which reflects variations in microvessel density [11–13]. Apparent diffusion coefficient (ADC) is derived from DWI and reflects changes in tissue structure [14–16].

Preliminary studies have demonstrated differences in metabolic parameters between high- and low-grade gliomas [17] but did not attempt to evaluate differences between subtypes of grade 2 gliomas. Although most grade 2 lesions have limited gadolinium enhancement, grade 2 oligodendrogliomas have been reported to have significantly higher maximum rCBV than grade 2 astrocytomas [18]. Evaluation of whole tumor ADC histograms [19] or ADC from tumor lesions [20] indicated that there are also differences in ADC between grade 2 oligodendrogliomas and astrocytomas. However, there have been few efforts so far to combine information from MRSI, PWI, and DWI to characterize subtypes of grade 2 gliomas. In the current study, we have expanded on previous work by investigating the characteristics of grade 2 gliomas in a larger population of patients using multiparametric MR imaging. The purpose was to determine whether the combination of metabolic, perfusion, and diffusion data could be helpful in targeting routine tissue sampling and hence augment the assessment of histologic subtypes for grade 2 gliomas.

Materials and Methods

Patients

Fifty-six patients with newly diagnosed grade 2 glioma according to the World Health Organization who had been scanned 1 day before surgery were selected for this study, including 24 with oligodendrogliomas (10 females and 14 males; median age, 43 years; range, 21-71 years), 18 with astrocytomas (7 females and 11 males; median age, 33.5 years; range, 22-52 years), and 14 with oligoastrocytomas (5 females and 9 males; median age, 45 years; range, 18-62 years). The ADC values for a subset of this patient population had been reported in a previous study [20], but the correlation of these data with other imaging parameters had not been considered. Informed consent to participate in the study was obtained using a protocol that had been reviewed and approved by the committee on human research at our institution. The clinical diagnosis was made by an experienced neuropathologist. For consensus diagnosis, a second neuropathologist independently reviewed all cases, and special stains were performed as necessary. Tumors that were classified as oligodendroglioma demonstrated the hallmark histopathologic features as defined by the World Health Organization's criteria [1].

MR Protocol

MR imaging was performed on a 1.5-T GE scanner (GE Medical Systems, Milwaukee, WI) equipped with a standard quadrature head coil. Anatomic T2-weighted three-dimensional fast spin-echo (FSE) image (time to repetition [TR]/time to echo [TE] = 4000/104 milliseconds, field of view [FOV] = 260 × 195 mm^2) and T1-weighted pre- and post-gadolinium three-dimensional spoiled gradient-echo images (TR/TE = 34/3 milliseconds, flip angle = 40°, FOV = 260 × 195 mm^2) were obtained from all patients. MRSI data were obtained from 47 of 56 patients using a three-dimensional chemical shift imaging multivoxel sequence and point-resolved spectral selection volume selection to cover as much of the lesion and surrounding normal tissue as possible. Imaging parameters were as follows: TR/TE = 1000/144 milliseconds, voxel size = 1 ml, phase-encoding arrays = 12 × 12 × 8 or 16 × 16 × 8. The acquisition of DWI in all 56 patients included either three gradient directions or six gradient directions (TR/TE = 1000/110 milliseconds, matrix size = 256 × 256, low/high b value = 5/1000 sec/mm^2, slice number/thickness = 28/3-5 mm). The PWI was obtained from 54 of 56 patients during injection of a bolus of 0.1-mmol/kg body weight of gadopentetate dimeglumine (Gd-DTPA) contrast agent at a rate of 5 ml/sec. A series of 60 T2*-weighted gradient-echo, echo-planar images were acquired during the first pass of the contrast agent bolus injection (TR/TE = 1000-1250/54 milliseconds, flip angle = 35°, matrix size = 128 × 128, slice number/thickness = 8/3-6 mm).

Data Processing

T2-weighted FSE and T1-weighted postcontrast images were first reformatted to create corresponding volume images. The T2-weighted FSE images were aligned to the T1-weighed postcontrast images using a rigid body surface matching method [21], whereas the PWI and DWI images were aligned using a rigid body mutual information algorithm [22]. Three-dimensional regions of interest (ROIs) corresponding to the hyperintensity region on T2-weighted FSE images (T2ALL) were delineated using an in-house semiautomatic program. The T1-weighted postcontrast images were examined to see if there were contrast-enhancing lesions in the T2ALL, which occurred in 6 of 56 patients, and the nonenhancing region was contoured as NEL = T2ALL – CEL. The ROIs of NEL were saved and transferred to metabolite, rCBV, and ADC maps for subsequent intensity analysis. ROIs were also drawn within normal-appearing white matter (NAWM) for use in normalizing rCBV maps.

The spectroscopy data were reconstructed to create a three-dimensional array of spectra from voxels on a regularly spaced grid using the method proposed previously [23]. Voxels that contain more than 50% of NEL and 75% NAWM were identified as tumor and normal voxels, respectively. Median intensities of choline (Cho), creatine (Cre), and *N*-acetyl aspartate (NAA) were determined from tumor voxels and were normalized by median values of normal voxels in the same patient. The Cho-to-NAA index (CNI) was estimated based on the differences in relative peak heights between tumor and normal tissues [24]. Briefly, an iterative algorithm is used to select a population of voxels that have the spectral features of normal brain regions; then the selected voxels are used as internal controls to quantify the probability of abnormality at each voxel location. Measures of the spatial extent of the metabolic lesions were obtained by considering the number of voxels that had CNI values greater than 2 or 3.

Perfusion images were resampled to a 32 × 32 in-plane grid so that the observed signal changes had sufficient signal-to-noise ratio to be

analyzed reliably on a voxel-by-voxel basis. The change of T2* signal intensity over time were processed to produce a map of rCBV [25]. Diffusion images were processed to generate ADC maps using an in-house program based on the mutilinear regression method from Basser et al. [26]. The mean, median, 25th percentile, and 75th percentile signal intensities of ADC and rCBV within NEL were recorded for each patient. Normalized rCBV values were obtained by dividing the calculated values from NEL by median values from NAWM.

Statistical Analysis

The nonparametric Wilcoxon rank sum test was used to evaluate differences among groups. Multiple comparisons between groups were corrected by using the Bonferroni method. Univariate logistic regression analysis was applied to quantify the contribution of each individual variable to discriminate the tumor subtypes. Multivariate logistic regression analysis was performed to determine whether the combinations of these variables could further improve the discrimination. The cutoff probability for the classification of subtypes in logistic regression analyses was set at 0.5. To evaluate the accuracy of the models for prediction, the probability of a lesion being in one *versus* the other subtype was estimated from the model and the lesion was assigned to the group for which the probability was higher. This probability estimate is conditional on the proportion of cases of each type in the sample. When the correlation between two variables was calculated, it referred to partial correlation adjusted by tumor subtype. The level of significance of difference was defined by a P value <.05. In the case of performing the Bonferroni correction, statistical significance was defined as $P < .05/k$, where k is the number of total comparisons. Statistical analysis was performed using SPSS (SPSS, Chicago, IL).

Results

All 56 patients had regions of hyperintensity on the T2-weighted images and 6 of them had regions of contrast enhancement on T1-weighted postcontrast images. The median tumor volume was 40 ml for patients with oligodendroglioma (range, 4-257 ml; contrast-enhancing $n = 3$), 39 ml for patients with astrocytoma (range, 10-160 ml; contrast-enhancing $n = 1$), and 55 ml for patients with oligoastrocytoma (range, 1-114 ml; contrast-enhancing $n = 2$). As can be seen, although the median lesion volumes were similar among subtypes, the large ranges indicated that the volumes were highly variable within each subgroup.

Figures 1, 2, and 3 show representative examples of the data from patients with grade 2 oligodendroglioma, astrocytoma, and oligoastrocytoma, respectively. Note that the ADC is elevated in the tumor relative to NAWM for all three patients, but the lesion from the patient with astrocytoma appears to have higher ADC than the lesions from the patients with oligodendroglioma and oligoastrocytoma. The patient with oligodendroglioma has a region on its rCBV map within the lesion that has higher rCBV values than NAWM. All three patients had voxels with reduced NAA and substantially elevated Cho relative to normal.

Evaluation of rCBV and ADC Values for Tumor Subtypes

All measurements of rCBV and ADC showed similar statistical significance in group comparisons. The median ADC and 75th percentile rCBV were chosen to be representative of results. The 75th percentile rCBV was chosen because it represents the most abnormal portion of the tumor and also avoids having the significance of the data being driven by only a few voxels as would be the case if the max rCBV were used [18]. Table 1 shows the average of the 75th percentile rCBV and the median ADC for each subtype. Higher 75th percentile rCBV (2.16 ± 0.50) and lower median ADC ($1.21 \pm 0.15 \times 10^{-3}$ mm^2/sec) were observed in oligodendrogliomas compared with astrocytomas (75th percentile rCBV 1.38 ± 0.41; median ADC $1.52 \pm 0.20 \times 10^{-3}$ mm^2/sec). Oligoastrocytomas had 75th percentile rCBV (1.49 ± 0.44) and median ADC ($1.41 \pm 0.15 \times 10^{-3}$ mm^2/sec) values intermediate to those from oligodendrogliomas and astrocytomas. None of the PWI and DWI parameters were found to be significantly different between astrocytomas and oligoastrocytomas and so no further statistical analysis was performed between them.

Differences in rCBV and ADC for Oligodendrogliomas versus Astrocytomas

The differences in 75th percentile rCBV and median ADC between oligodendrogliomas and astrocytomas were significant ($P < .0001$ and $P < .00001$, respectively). The P values listed in Tables 1 and 4 are nominal P values unadjusted for multiple comparisons. Using the Bonferroni adjustment, comparisons would only be considered statistically significant if the nominal P value was less than $.0018 \approx .05/27$, where 27 was the total number of comparisons in Tables 1 and 4. Logistic regression analysis was performed for the patients who underwent both perfusion and diffusion studies. This included 22 patients with oligodendroglioma and 18 patients with astrocytoma. Table 2 gives the results from both univariate and bivariate logistic regression analyses. In univariate analysis, 77.5% (31/40) and 85% (34/40) of the patients were correctly classified using 75th percentile rCBV and median ADC, respectively. Of those being correctly classified patients by either 75th percentile rCBV or median ADC, 26 of them were correctly classified by both variables. When 75th percentile rCBV and median ADC were combined in a bivariate analysis, they were both significant variables ($P = .034$ for 75th percentile rCBV; $P = .012$ for median ADC), and 92.5% (37/40) of the patients were correctly classified.

Differences in rCBV and ADC for Oligodendrogliomas versus Oligoastrocytomas

A similar comparison between oligodendrogliomas and oligoastrocytomas showed that the differences in 75th percentile rCBV and median ADC between oligodendrogliomas and oligoastrocytomas were significant ($P < .001$ in both cases). The results from the analysis with logistic regression are shown in Table 3. The regression correctly classified 75% (27/36) of original grouped patients with the use of 75th percentile rCBV or median ADC alone. Of those being correctly classified patients by either the 75th percentile rCBV or the median ADC, 22 of them were correctly classified by both variables. Again the 75th percentile rCBV ($P = .031$) and median ADC ($P = .049$) were significant variables in bivariate analysis, and 83.3% (30/36) of the patients were correctly classified.

Metabolite Levels and Lesion Volumes

Table 4 gives metabolite levels and indices within the portion of NEL that was covered by the point-resolved spectral selection box. Oligodendrogliomas had higher median Cho (1.48 ± 0.57), Cre (0.95 ± 0.21), and NAA (0.48 ± 0.15) than astrocytomas (median Cho 1.19 ± 0.26; median Cre 0.83 ± 0.20; median NAA 0.40 ± 0.14) and oligoastrocytomas (median Cho 1.14 ± 0.19; median Cre 0.86 ± 0.11; median NAA 0.42 ± 0.12). These differences were not

significant due to the substantial variability in metabolite levels among patients within each subtype. The median numbers of voxels with CNI > 2 or CNI > 3, the median CNI for CNI > 2, and the median of the maximum CNI values did not change substantially between subtypes, but again there were large variations between different patients. Examples of differences in the metabolic lesions for two patients with oligodendroglioma are seen in Figure 4.

Correlations between Parameters

The 75th percentile rCBV and median ADC were inversely correlated with $R = -0.52$ ($P < .001$). The ADC values in the voxels with maximum CNI were correlated with the median ADC from NEL with $R = 0.70$ ($P < .001$). There was no correlation between the maximum CNI and ADC at the corresponding location or between the median CNI and median ADC from NEL.

Discussion

Accurate classification of grade 2 infiltrating gliomas and evaluation of tumor burden have important implications for diagnosis, prognosis, and selection of the most appropriate therapy. As was seen from the evaluation of anatomic images, most of these lesions are nonenhancing on T1-weighted postcontrast images and the lesions observed on T2-weighted images can be large, with relatively uniform intensity. This means that selecting the most appropriate region

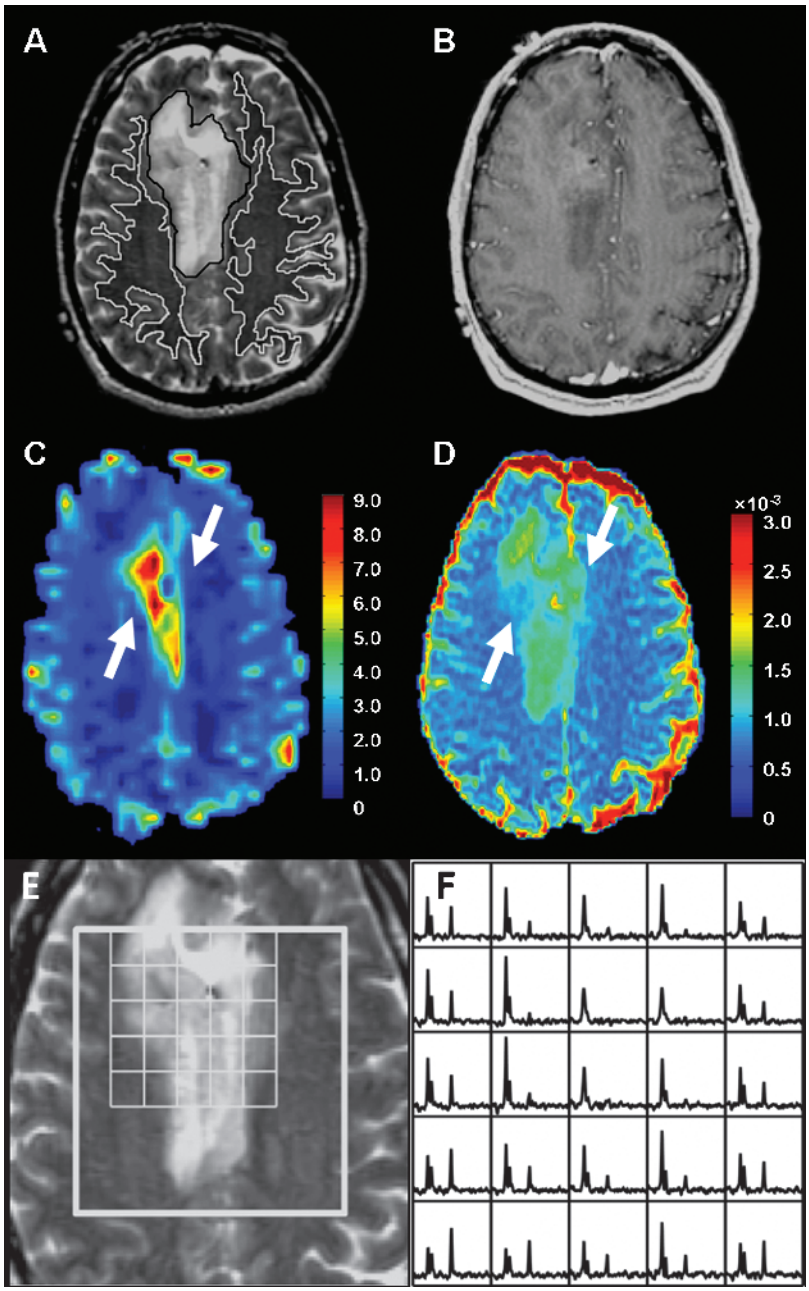

Figure 1. MR images and spectra from a patient with oligodendroglioma. (A) Axial T2-weighted FSE image with contours of T2ALL (black) and NAWM (white). (B) T1-weighted postcontrast image showing no contrast enhancement. (C) rCBV map showing a large focus of increased blood volume (arrows) in the tumor. (D) ADC map showing mildly increased magnitude of diffusion (arrows) in the tumor. (E and F) T2-weighted FSE image overlaid with arrays of spectra showing voxels with elevated Cho and reduced NAA peaks in the tumor.

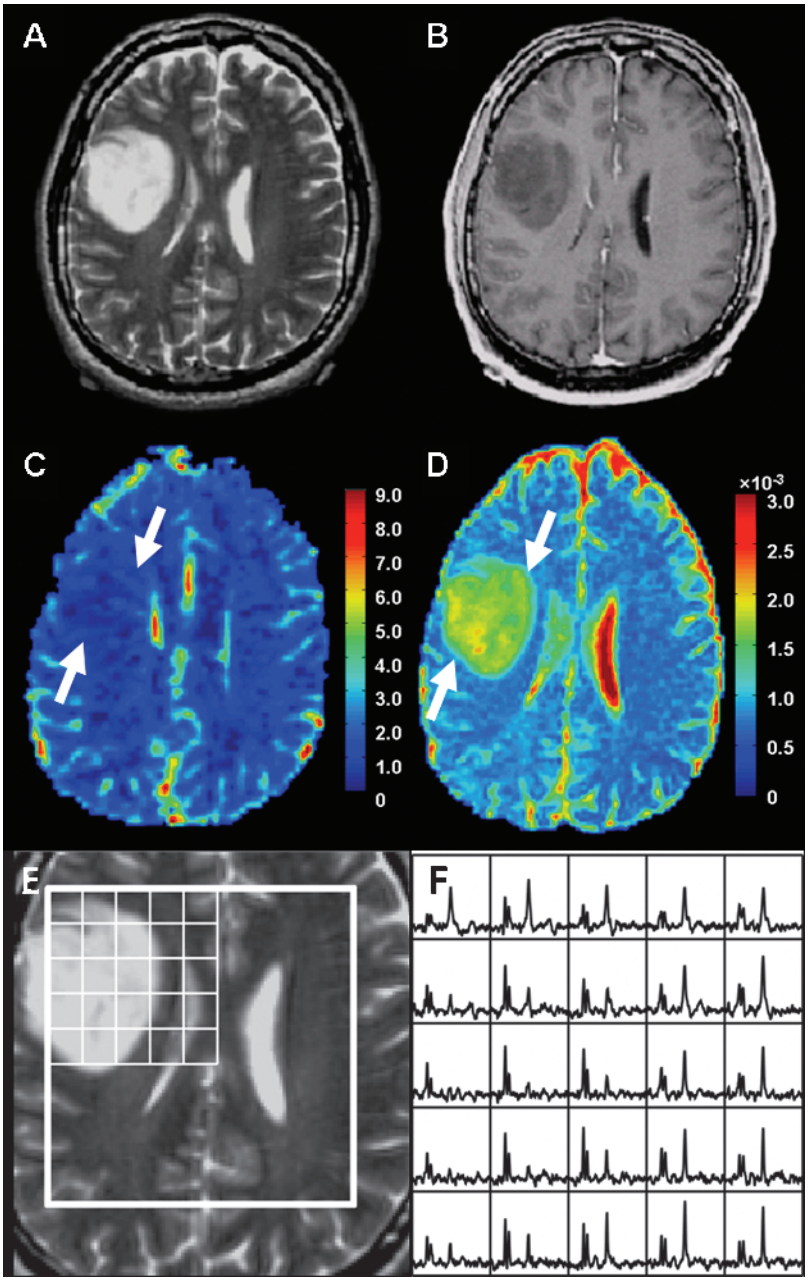

Figure 2. MR images and spectra from a patient with astrocytoma. (A) Axial T2-weighted FSE image. (B) T1-weighted postcontrast image showing no contrast enhancement. (C) rCBV map showing minimally increased blood volume (arrows) in the tumor. (D) ADC map showing a large focus of increased magnitude of diffusion (arrows) in the tumor. (E and F) T2-weighted FSE image overlaid with arrays of spectra showing voxels with elevated Cho and reduced NAA peaks in the tumor.

for tissue sampling to make an accurate diagnosis is problematic and would therefore benefit from having imaging information that distinguishes regions of the tumor with different physiological or metabolic characteristics. In the present study, we were interested in determining whether data from MRSI, PWI, and DWI could provide parameters that could be used for targeting tissue sampling and for providing information that would contribute to the characterization and therapeutic planning for patients with grade 2 glioma.

MRSI is a method that measures chemical markers of neoplastic activity. Spectra from brain tumors have increased Cho, which correlates with membrane biosynthesis by proliferating cells, and reduced NAA, which indicates loss of neuronal integrity due to tumor cell infiltration [8]. In this study, reduced NAA and increased Cho were found in all grade 2 glioma subtypes with a trend toward higher Cho in oligodendroglioma than in astrocytoma and oligoastrocytoma. This trend may be explained by the fact that oligodendrogliomas have been reported to be more proliferative than astrocytomas [27,28]. The varying levels of NAA that were observed in these lesions may be due to the limited spatial resolution of the MRSI data, which allows voxels on the edge of the tumor to include some normal brain tissue or to the heterogeneity within the tumor itself, which may include a mixture of infiltrative tumor and residual normal tissue. No significant differences in individual metabolite values were found between subtypes, which is consistent with previous studies [29–31].

The CNI is a quantitative parameter that describes the differences in Cho and NAA relative to normal tissue and that has been shown to be sensitive to the presence of tumor [32]. From our studies, it seems that obtaining a tissue sample from the region with highest CNI is likely to reveal the area with the highest density of tumor cells and lowest amount of normal brain. Thus, whereas there is an overlap between the CNI levels for different histologic subtypes, the highest CNI levels are observed in oligodendrogliomas and these *in vivo* measurements may be useful in directing a surgeon to the location that gives the most definitive histologic diagnosis. Previous studies that examined the correlation between metabolite levels and tissue biopsies have suggested that the ratio of Cho to NAA and the level of Cho relative to Cre in normal brain may be more effective in defining the borders of the tumor than the region of hyperintensity on T2-weighted images [33]. These values may also be important in postsurgical MR examinations for evaluating residual tumor or for assessing response to therapy. Although the echo time used in this study precluded the quantification of levels of glutamate, previous reports indicated that these may also be relevant in distinguishing grade 2 oligodendrogliomas from astrocytomas [30].

PWI provides measurements of rCBV that reflect tumor angiogenesis and vascularity. In our study, the 75th percentile rCBV of

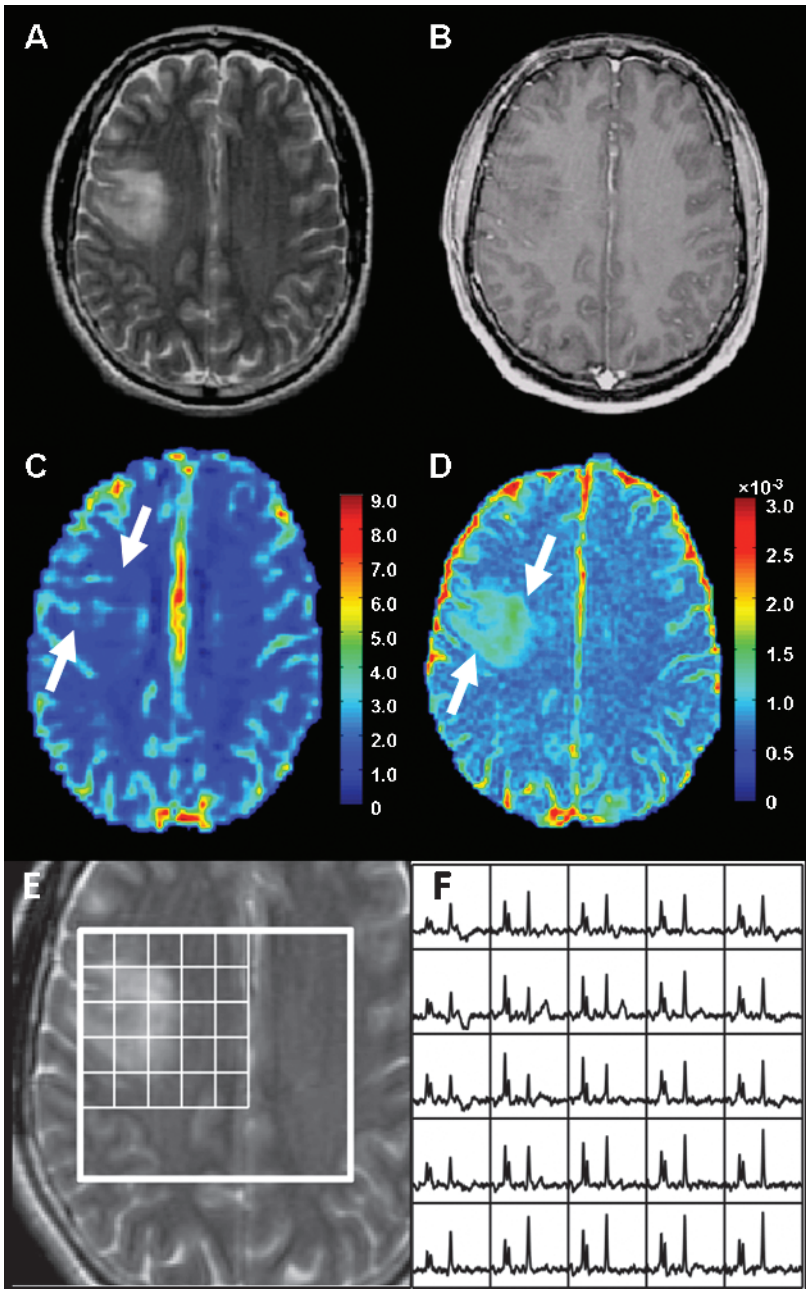

Figure 3. MR images and spectra from a patient with oligoastrocytoma. (A) Axial T2-weighted FSE image. (B) T1-weighted postcontrast image showing no contrast enhancement. (C) rCBV map showing mildly increased blood volume (arrows) in the tumor. (D) ADC map showing mildly increased magnitude of diffusion (arrows) in the tumor. (E and F) T2-weighted FSE image overlaid with arrays of spectra showing voxels with elevated Cho and reduced NAA peaks in the tumor.

Table 1. Average of Median ADC and the 75th Percentile rCBV in NEL for Each Grade 2 Glioma Subtype (Data Are Presented as Mean ± SD) and *P* Values from a Wilcoxon Rank Sum Test.

Parameter	OD	OA	AC	*P*: OD *vs* AC	*P*: OD *vs* OA	*P*: AC *vs* OA
Median ADC*,†	1.21 ± 0.15	1.41 ± 0.15	1.52 ± 0.20	**<.00001**	**<.001**	.106
75th percentile rCBV‡	2.16 ± 0.50	1.49 ± 0.44	1.38 ± 0.41	**<.0001**	**<.001**	.582

P values in bold face font indicate statistical significance.
AC indicates astrocytoma; *OA*, oligoastrocytoma; *OD*, oligodendroglioma (similar to Tables 2–4).
*MR diffusion cases: OD (*n* = 24), OA (*n* = 14), and AC (*n* = 18).
†Units of ADC are 10^{-3} mm^2/sec.
‡MR perfusion cases: OD (*n* = 22), OA (*n* = 14), and AC (*n* = 18).

oligodendrogliomas was significantly higher than the value for astrocytomas or oligoastrocytomas. This difference may be explained by the fact that oligodendrogliomas are more likely to exhibit microvascular proliferation than the astrocytomas and oligoastrocytomas [34,35]. Statistical analysis showed that the 75th percentile rCBV was a significant variable in the differentiation of oligodendrogliomas from each of the other two subtypes. These results confirm observations from a previous study in a smaller population of patients, which found that the maximum rCBV within the tumor was significantly higher for oligodendrogliomas than for astrocytomas [18].

ADC values derived from diffusion MR imaging provide a measurement of the movement of water molecules within tissue microstructures. Although ADC is thought to correlate to cell density in high-grade tumors [16], both the results of this study and the observations made in previous studies have indicated that there is no clear correlation between ADC and levels of Cho for grade 2 gliomas [17,36]. One explanation of this is that the levels of ADC observed in these lesions are also influenced by other biologic factors, such as the presence of edema and calcification. Edema represents an increase of free extracellular water content of tissue and should therefore result in a higher ADC [37,38]. It is reasonable to expect that there would be more edema in astrocytomas than oligodendrogliomas because they are more infiltrative. Calcification is more common in oligodendrogliomas [39] and results in a relatively lower ADC because it limits water content and restricts water movement. The values for oligodendrogliomas that were observed in this study are in agreement with previous data, which use the analysis of whole-tumor ADC histograms [19].

The classification accuracy of the logistic regression model based on median ADC was higher than that based on the 75th percentile rCBV. When they were both included in the regression, the accuracy showed a slight improvement over median ADC alone, with 3 of 40 additional patients for the analysis of oligodendrogliomas *versus* astrocytomas and 3 of 36 additional patients for the analysis of oligodendrogliomas *versus* oligoastrocytomas being correctly classified. The similarity in classification between the two variables was most likely due to the 75th percentile rCBV and the median ADC being inversely correlated, which indicates that increased vascularity and restricted diffusion were present in a coordinated fashion. It should be noted that there are limitations on these assessments based on the logistic models. First, the classification accuracy of the model is being evaluated using the same data set used to create the model. This will tend to overestimate the ability of the model to predict for an independent set of cases. In addition, by setting the cutoff probability to be 0.5, we assume that the proportion of cases with the specified subtypes would accurately represent the proportions seen in the general population of cases. Even with these caveats, the results provide strong evidence that both the 75th percentile rCBV and the median ADC provide useful information for distinguishing oligodendrogliomas from astrocytomas and oligoastrocytomas.

Oligoastrocytomas contain variable proportions of cell populations that display both astrocytic and oligodendroglial phenotypes [1]. The MR findings obtained in our study reflected the mixed cellular phenotypes of these tumors in that they had 75th percentile rCBV and median ADC values that fell in between those of oligodendrogliomas and astrocytomas. It should be noted that although our results are consistent with several other studies that have reported on differences in imaging characteristics for grade 2 gliomas, the histologic criteria for distinguishing oligoastrocytomas from oligodendrogliomas and astrocytomas may vary between institutions. Low-grade gliomas display a broad range of cellular phenotypes, with the classic oligodendrogliomas and astrocytomas being at different ends of a discontinuous spectrum [40]. It is therefore possible that some of the patients whom we defined as having oligoastrocytoma would have been diagnosed as having oligodendroglioma or astrocytoma in other institutions. For the purposes of our study, we focused on identifying only those tumors with hallmark histopathologic features as oligodendrogliomas, whereas the criteria used to separate oligoastrocytomas and astrocytomas were less distinctive. It is therefore not surprising that these two subpopulations had similar features and could not be distinguished based on the MR parameters considered.

One of the limitations of the current study is that we were unable to make a direct link between the MR imaging parameters and the histologic examinations because the sample used for diagnosis was not targeted based on metabolic and physiological imaging data. Thus, although the MR findings from this study were attributed

Table 2. Number of Correct Assignments Using the 75th Percentile rCBV, Median ADC, and Their Combination in the Differentiation of Oligodendrogliomas from Astrocytomas.

	OD and AC (%)	OD (%)	AC (%)
75th percentile rCBV*	31/40 (77.5)	18/22 (81.8)	13/18 (72.2)
Median ADC*	34/40 (85.0)	19/22 (86.4)	15/18 (83.3)
75th percentile rCBV + median ADC†	37/40 (92.5)	20/22 (90.9)	17/18 (94.4)

*Univariate analysis.
†Bivariate analysis.

Table 3. Number of Correct Assignments Using the 75th Percentile rCBV, Median ADC, and Their Combination in the Differentiation of Oligodendrogliomas from Oligoastrocytomas.

	OD and OA (%)	OD (%)	OA (%)
75th percentile rCBV*	27/36 (75.0)	18/22 (81.8)	9/14 (64.3)
Median ADC*	27/36 (75.0)	19/22 (86.4)	8/14 (57.1)
75th percentile rCBV + median ADC†	30/36 (83.3)	20/22 (90.9)	10/14 (71.4)

*Univariate analysis.
†Bivariate analysis.

Table 4. Summary of Parameters from MRSI in NEL for Each Grade 2 Glioma Subtype and *P* Values from a Wilcoxon Rank Sum Test.

Parameter	OD, *n* = 20	OA, *n* = 12	AC, *n* = 15	*P*: OD *vs* AC	*P*: OD *vs* OA	*P*: AC *vs* OA
Median Cho*	1.48 ± 0.57	1.14 ± 0.19	1.19 ± 0.26	.178	.155	.757
Median Cre	0.95 ± 0.21	0.86 ± 0.11	0.83 ± 0.20	.093	.124	.757
Median NAA	0.48 ± 0.15	0.42 ± 0.12	0.40 ± 0.14	.066	.227	.857
No. of voxels with CNI > 2†	24	27.5	20	.652	.922	.751
	5-160	10-46	4-53			
No. of voxels with CNI > 3	8.5	12	9	.987	.984	.807
	0-129	0-25	1-37			
Median CNI for CNI > 2 voxels	3.02	2.89	3.03	.665	.586	.643
	2.23-6.1	2.18-3.94	2.17-3.69			
Max CNI	5.91	5.48	5.11	.217	.425	.510
	2.47-16.78	2.87-7.66	3.04-8.22			

*Numbers are median ± SD.
†Numbers are median and range.

to histopathologic factors such as neoangiogenesis, cell density, presence of edema, and calcification, we cannot be certain as to the contribution that each individual factor makes to each measurement. Further studies that directly correlate imaging with histologic observations will be important for enhancing the interpretation of MR-derived parameters. We recommend targeting locations within the region of T2 hyperintensity with the highest CNI value, elevated rCBV, or ADC values in the ranges that were found to be indicative of oligodendrogliomas or astrocytomas. Note that there was a direct correlation between ADC values at the location with maximum CNI with the median ADC values. This indicates that targeting the region with the most abnormal metabolism should provide representative data for the entire tumor.

Another factor that may be important for future studies is to use recent advances in genetics to develop more accurate and prognostically relevant tumor classification systems. Reports based on molecular biology of gliomas have suggested that loss of heterozygosity chromosomes 1p and 19q is typical of oligodendrogliomas, whereas mutation of *TP53* gene is far more likely to associate with astrocytomas [5,41,42]. These findings have increased the interest in

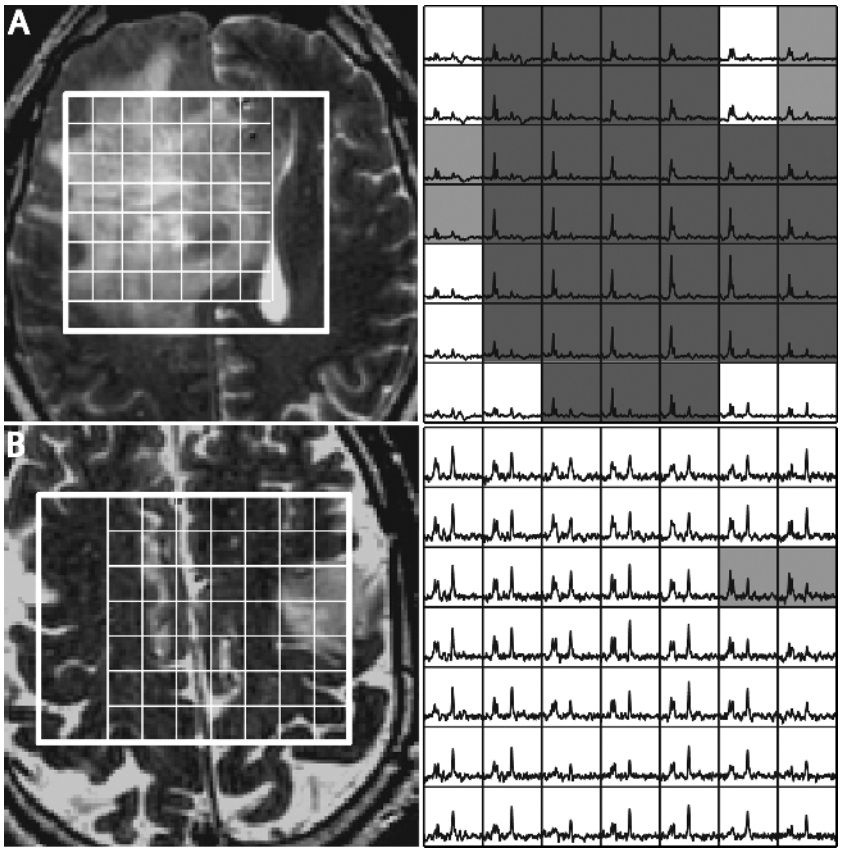

Figure 4. T2-weighted FSE images (left) and spectra (right) from two patients who had oligodendrogliomas but with a different number of voxels with elevated CNI. Voxels highlighted in light gray have CNI > 2 and voxels highlighted in dark gray have CNI > 3. Patient A had 160 voxels with CNI > 2, 129 voxels with CNI > 3, and the max CNI = 16.8. Patient B had 10 voxels with CNI > 2, no voxels with CNI > 3, and the max CNI = 2.9.

investigating the relationship among MR imaging findings, glioma genotype, and histologic type [31,43–45]. By performing these correlation studies, it will be possible to develop more definitive reference standards for glioma subtypes and to validate the use of MR imaging parameters as noninvasive biomarkers for directing surgical sampling, evaluating tumor burden, and assessing response to therapy.

Conclusions

The results of this study showed that PWI and DWI were useful in differentiating grade 2 oligodendroglioma from grade 2 astrocytomas and oligoastrocytomas. The variations in maximum CNI and the number of voxels with abnormal CNI indicate that there is a much larger range of values in the oligodendrogliomas than for the other histologic subtypes. Using these imaging methods to target tissue sampling may be valuable in overcoming some of the limitations associated with histopathologic examinations and may contribute to designing the treatment plan that best matches the characteristics of the tumor. These observations may also be valuable for targeting therapy, evaluating residual disease, and assessing response to therapy.

Acknowledgments

The authors thank Ying Lu, Tracy R. McKnight, and Qian Zhao for useful discussions and assistance with the interpretation of the data.

References

[1] Louis DN, Ohgaki H, Wiestler OD, and Cavenee WK (2007). *WHO Classification of Tumours of the Central Nervous System.* Lyon, France: IARC Press.

[2] Mason WP, Krol GS, and DeAngelis LM (1996). Grade II oligodendroglioma responds to chemotherapy. *Neurology* **46**, 203–207.

[3] Leighton C, Fisher B, Bauman G, Depiero S, Stitt L, MacDonald D, and Cairncross G (1997). Supratentorial grade II glioma in adults: an analysis of prognostic factors and timing of radiation. *J Clin Oncol* **15**, 1289–1290.

[4] Perry JR, Louis DN, and Cairncross JG (1999). Current treatment of oligodendrogliomas. *Arch Neurol* **56**, 434–436.

[5] Sasaki H, Zlatescu MC, Betensky RA, Johnk LB, Cutone AN, Cairncross JG, and Louis DN (2002). Histopathological-molecular genetic correlations in referral pathologist-diagnosed grade II "oligodendroglioma". *J Neuropathol Exp Neurol* **61**, 58–63.

[6] Dean BL, Drayer BP, Bird CR, Flom RA, Hodak JA, Coons SW, and Carey RG (1990). Gliomas: classification with MR imaging. *Radiology* **174**, 411–415.

[7] Cha S (2006). Update on brain tumor imaging: from anatomy to physiology. *AJNR Am J Neuroradiol* **27**, 475–487.

[8] Lee PL and Gonzalez RG (2000). Magnetic resonance spectroscopy of brain tumors. *Curr Opin Oncol* **12**, 199–204.

[9] Vigneron D, Bollen A, McDermott M, Wald L, Day M, Moyher-Noworolski S, Henry R, Chang S, Berger M, Dillon W, et al. (2001). Three-dimensional magnetic resonance spectroscopic imaging of histologically confirmed brain tumors. *Magn Reson Imaging* **19**, 89–101.

[10] Nelson SJ (2003). Multivoxel magnetic resonance spectroscopy of brain tumors. *Mol Cancer Ther* **2**, 497–507.

[11] Sugahara T, Korogi Y, Kochi M, Ikushima I, Hirai T, Okuda T, Shigematsu Y, Liang L, Ge Y, Ushio Y, et al. (1998). Correlation of MR imaging–determined cerebral blood volume maps with histologic and angiographic determination of vascularity of gliomas. *AJR Am J Roentgenol* **171**, 1479–1486.

[12] Petrella JR and Provenzale JM (2000). MR perfusion imaging of the brain: techniques and applications. *AJR Am J Roentgenol* **175**, 207–219.

[13] Cha S, Knopp EA, Johnson G, Wetzel SG, Litt AW, and Zagzag D (2002). Intracranial mass lesions: dynamic contrast-enhanced susceptibility-weighted echo-planar perfusion MR imaging. *Radiology* **223**, 11–29.

[14] Basser PJ and Pierpaoli C (1996). Microstructural and physiological features of tissues elucidated by quantitative-diffusion-tensor MRI. *J Magn Reson B* **11**, 209–219.

[15] Brunberg JA, Chenevert TL, McKeever PE, Ross DA, Junck LR, Muraszko KM, Dauser R, Pipe JG, and Betley AG (1995). *In vivo* MR determination of water diffusion coefficients and diffusion anisotropy: correlation with structural alteration in gliomas of the cerebral hemispheres. *AJNR Am J Neuroradiol* **16**, 361–371.

[16] Sugahara T, Korogi Y, Kochi M, Ikushima I, Shigematu Y, Hirai T, Okuda T, Liang L, Ge Y, Komohara Y, et al. (1999). Usefulness of diffusion-weighted MRI with echo-planar technique in the evaluation of cellularity in gliomas. *J Magn Reson Imaging* **9**, 53–60.

[17] Catalaa I, Henry R, Dillon WP, Graves EE, McKnight TR, Lu Y, Vigneron DB, and Nelson SJ (2006). Perfusion, diffusion and spectroscopy values in newly diagnosed cerebral gliomas. *NMR Biomed* **19**, 463–475.

[18] Cha S, Tihan T, Crawford F, Fischbein NJ, Chang S, Bollen A, Nelson SJ, Prados M, Berger MS, and Dillon WP (2005). Differentiation of grade II oligodendrogliomas from grade II astrocytomas by using quantitative blood-volume measurements derived from dynamic susceptibility contrast-enhanced MR imaging. *AJNR Am J Neuroradiol* **26**, 266–273.

[19] Tozer DJ, Jäger HR, Danchaivijitr N, Benton CE, Tofts PS, Rees JH, and Waldman AD (2007). Apparent diffusion coefficient histograms may predict grade II glioma subtype. *NMR Biomed* **20**, 49–57.

[20] Khayal IS, McKnight TR, McGue C, Vandenberg S, Lamborn KR, Chang SM, Cha S, and Nelson SJ (2009). Apparent diffusion coefficient and fractional anisotropy of newly diagnosed grade II gliomas. *NMR Biomed* **22**, 449–455.

[21] Nelson SJ, Nalbandian AB, Proctor E, and Vigneron DB (1994). Registration of images from sequential MR examinations of the brain. *J Magn Reson Imaging* **4**, 877–883.

[22] Studholme C, Hill DLG, and Hawkes D (1999). An overlap invariant entropy measure of 3D medical image alignment. *Pattern Recogn* **32**, 71–86.

[23] Nelson SJ (2001). Analysis of volume MRI and MR spectroscopic imaging data for the evaluation of patients with brain tumors. *Magn Reson Med* **46**, 228–239.

[24] McKnight TR, Noworolski SM, Vigneron DB, and Nelson SJ (2001). An automated technique for the quantitative assessment of 3D-MRSI data from patients with glioma. *J Magn Reson Imaging* **13**, 167–177.

[25] Lupo JM, Lee MC, Han ET, Cha S, Chang SM, Berger MS, and Nelson SJ (2006). Feasibility of dynamic susceptibility contrast perfusion MR imaging at 3T using a standard quadrature head coil and eight-channel phased-array coil with and without SENSE reconstruction. *J Magn Reson Imaging* **24**, 520–529.

[26] Basser PJ, Mattiello J, and LeBihan D (1994). Estimation of the effective self-diffusion tensor from the NMR spin echo. *J Magn Reson B* **103**, 247–254.

[27] Heesters MA, Koudstaal J, Go KG, and Molenaar WM (1999). Analysis of proliferation and apoptosis in brain gliomas: prognostic and clinical value. *J Neurooncol* **44**, 255–266.

[28] Schiffer D, Cavalla P, Dutto A, and Borsotti L (1997). Cell proliferation and invasion in malignant gliomas. *Anticancer Res* **17**, 61–69.

[29] Croteau D, Scarpace L, Hearshen D, Gutierrez J, Fisher JL, Rock JP, and Mikkelsen T (2001). Correlation between magnetic resonance spectroscopy imaging and image-guided biopsies: semiquantitative and qualitative histopathological analyses of patients with untreated glioma. *Neurosurgery* **49**, 823–829.

[30] Rijpkema M, Schuuring J, van der Meulen Y, van der Graaf M, Bernsen H, Boerman R, van der Kogel A, and Heerschap A (2003). Characterization of oligodendrogliomas using short echo time ^{1}H MR spectroscopic imaging. *NMR Biomed* **16**, 12–18.

[31] Jenkinson MD, Smith TS, Joyce K, Fildes D, du Plessis DG, Warnke PC, and Walker C (2005). MRS of oligodendroglial tumors: correlation with histopathology and genetic subtypes. *Neurology* **28**, 2085–2089.

[32] McKnight TR, von dem Bussche MH, Vigneron DB, Lu Y, Berger MS, McDermott MW, Dillon WP, Graves EE, Pirzkall A, and Nelson SJ (2002). Histopathological validation of a three-dimensional magnetic resonance spectroscopy index as a predictor of tumor presence. *J Neurosurg* **97**, 794–802.

[33] McKnight TR, Lamborn KR, Love TD, Berger MS, Chang S, Dillon WP, Bollen A, and Nelson SJ (2007). Correlation of magnetic resonance spectroscopic and growth characteristics within grades II and III gliomas. *J Neurosurg* **106**, 660–666.

[34] Christov C and Gherardi RK (1999). Vascular endothelial growth factor (VEGF) likely contributes to oligodendroglioma angiogenesis. *Acta Neuropathol* **97**, 429–432.

[35] Schiffer D, Bosone I, Dutto A, Di Vito N, and Chiò A (1999). The prognostic role of vessel productive changes and vessel density in oligodendroglioma. *J Neurooncol* **44**, 99–107.

[36] Khayal IS, Crawford FW, Saraswathy S, Lamborn KR, Chang SM, Cha S, McKnight TR, and Nelson SJ (2008). Relationship between choline and apparent diffusion coefficient in patients with gliomas. *J Magn Reson Imaging* **27**, 718–725.

[37] Krabbe K, Gideon P, Wagn P, Hansen U, Thomsen C, and Madsen F (1997). MR diffusion imaging of human intracranial tumours. *Neuroradiology* **39**, 483–489.
[38] Lu S, Ahn D, Johnson G, Law M, Zagzag D, and Grossman RI (2004). Diffusion-tensor MR imaging of intracranial neoplasia and associated peritumoral edema: introduction of the tumor infiltration index. *Radiology* **232**, 221–228.
[39] Rees JH (2002). Grade II gliomas in adults. *Curr Opin Neurol* **15**, 657–661.
[40] Cillekens JM, Beliën JA, van der Valk P, Faes TJ, van Diest PJ, Broeckaert MA, Kralendonk JH, and Kamphorst W (2000). A histopathological contribution to supratentorial glioma grading, definition of mixed gliomas and recognition of low grade glioma with Rosenthal fibers. *J Neurooncol* **46**, 23–43.
[41] Reifenberger G and Louis DN (2003). Oligodendroglioma: toward molecular definitions in diagnostic neuro-oncology. *J Neuropathol Exp Neurol* **62**, 111–126.
[42] Ohgaki H and Kleihues P (2005). Population-based studies on incidence, survival rates, and genetic alterations in astrocytic and oligodendroglial gliomas. *J Neuropathol Exp Neurol* **64**, 479–489.
[43] Jenkinson MD, Smith TS, Joyce KA, Fildes D, Broome J, du Plessis DG, Haylock B, Husband DJ, Warnke PC, and Walker C (2006). Cerebral blood volume, genotype and chemosensitivity in oligodendroglial tumours. *Neuroradiology* **48**, 703–713.
[44] Whitmore RG, Krejza J, Kapoor GS, Huse J, Woo JH, Bloom S, Lopinto J, Wolf RL, Judy K, Rosenfeld MR, et al. (2007). Prediction of oligodendroglial tumor subtype and grade using perfusion weighted magnetic resonance imaging. *J Neurosurg* **107**, 600–609.
[45] Jenkinson MD, Smith TS, Brodbelt AR, Brodbelt AR, Joyce KA, Warnke PC, and Walker C (2007). Apparent diffusion coefficients in oligodendroglial tumors characterized by genotype. *J Magn Reson Imaging* **26**, 1405–1412.